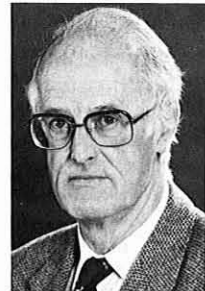


A Semi-Empirical Model for Dynamic Stall



J. G. Leishman*
Senior Aerodynamicist



T. S. Beddoes
Aerodynamics Specialist

Aerodynamics Department
Westland Helicopters Ltd.
Yeovil, England

A semi-empirical model is formulated to represent the unsteady lift, drag, and pitching moment characteristics of an airfoil undergoing dynamic stall. The model is presented in a form which is consistent with an indicial formulation for the unsteady aerodynamics under attached flow conditions. The onset of vortex shedding during dynamic stall is represented using a criterion for leading edge or shock induced separation based on the attainment of a critical leading edge pressure. The induced vortex lift is represented empirically along with the associated pitching moment which is obtained by allowing the center of pressure to move in a time dependent manner during dynamic stall. Significant nonlinearities in the airfoil behavior associated with trailing edge separation are represented using a Kirchhoff flow model in which the separation point is related to the airfoil behavior. These effects are represented in such a way as to allow progressive transition between the dynamic stall and the static stall characteristics. It is shown how the above features may be implemented as an algorithm suitable for inclusion within rotorcraft airloads or aeroelasticity analyses. Validation of the model is presented with force and moment data from two-dimensional unsteady tests on the NACA 0012, HH-02, and SC-1095 airfoils.

Nomenclature

a	= Sonic velocity, m/s	C_p	= Pressure coefficient
A_i	= Coefficients of indicial response function	C_v	= Vortex lift increment
b_i	= Exponents of indicial response function	C_w	= Work per cycle coefficient = $-\oint C_M d\alpha$
c	= Airfoil chord, m	D, D_p, D_f	= Deficiency functions
C_c	= Chord force coefficient	f	= Trailing edge separation point
C_D	= Pressure drag coefficient	k	= Reduced frequency = $\omega_c/2V$
C_{D_0}	= Zero lift (viscous) drag coefficient	K	= Noncirculatory time constant multiplier
C_M	= 1/4-chord pitching moment coefficient	K_0, K_1, K_2	= Coefficients representing pitching moment curve fit
C'_M	= Vortex induced pitching moment coefficient	M	= Mach number
C_N	= Normal force coefficient	n	= Current time sample
C'_{N_1}	= Critical normal force coefficient delimiting attached flow	S	= Nondimensional distance traveled by airfoil in semi-chords = $2Vt/c$
C_N^c	= Circulatory normal force coefficient	S_1, S_2	= Coefficients of separation point curve fit
C'_N	= Noncirculatory (impulsive) normal force coefficient	St	= Strouhal number
C_N^p	= Normal force under potential flow conditions	t	= Time, s
C'_N	= Vortex induced normal force coefficient	T_I	= Noncirculatory time constant = c/a
C_{N_a}	= Normal force (lift) curve slope, rad	T_p, T_f, T_v, T_{St}	= Time constants (semi-chords)
$C_{N_{MAX}}$	= Maximum normal force coefficient	T_{vl}	= Vortex passage time constant
CP_v	= Vortex induced center of pressure	V	= Free stream velocity, m/s
		x	= Nondimensional chord
		x_{ac}	= Aerodynamic center
		X, Y	= Circulatory deficiency functions
		α	= Angle of attack, deg
		α_E	= Effective angle of attack, deg
		β	= Prandtl-Glauert compressibility factor = $\sqrt{1 - M^2}$

*Currently Assistant Professor, Department of Aerospace Engineering, University of Maryland.

Revised version of a paper presented at the 42nd Annual Forum of the American Helicopter Society, Washington, D.C., Jun 1986.

- τ_v = Nondimensional vortex time
- ϕ = Indicial response function
- η = Chordwise force recovery factor
- ω = Circular frequency, rad/s

Introduction

The successful design of advanced rotorcraft requires the ability to confidently predict the large unsteady and vibratory loads generated and transmitted by the rotor system. The capability to accomplish this has improved significantly in recent years as a result of advances in the analytical modeling of blade structural dynamics, the rotor wake geometry, and unsteady aerodynamics. While structural dynamic modeling has now reached a good level of maturity, the development of accurate and computationally efficient aerodynamic models that represent the unsteady behavior of the blade sections still poses a major challenge to the rotor analyst. Generally, the analyst needs to determine an appropriate compromise between the accuracy of a given aerodynamic model and the need to keep computational requirements within practical limits. In many circumstances, these requirements are conflicting and the rotor analyst is often forced to resort to a relatively simple quasi-steady representation for the aerodynamics. Unfortunately, this can restrict the range of flight conditions over which the analysis can be applied, and thereby severely limit its generality as a practical design tool.

Within a helicopter rotor flow field, the blades encounter complex time varying changes in aerodynamic angle of attack due to imposed control inputs, the dynamic motion of the blades, and large local variations in inflow velocity that arise from the complex three-dimensional vortex wake system. In many rotor

operating regimes, unsteady aerodynamic effects are of low magnitude and can be justifiably neglected in any analysis. However, if the angle of attack of the blade sections becomes large enough, dynamic stall may occur. Typically, this occurs on the retreating blade under conditions of high blade loading and in high speed forward flight. The rotor operational limitations (i.e., vibration, aeroelastic stability, maximum control loads and fatigue limits) are all determined by the onset of transient flow separation such as dynamic stall.

Many experimental tests (Refs. 1-5) have shown that the distinguishing feature of dynamic stall compared with static stall is the shedding of significant concentrated vorticity from the airfoil leading-edge region. This vortex disturbance is subsequently swept over the airfoil chord and induces a strong moving pressure wave on the airfoil surface. These pressure changes result in significant increases in airfoil lift and in large nose-down pitching moments well in excess of the static values. A typical example is illustrated in Fig. 1 which also identifies the main features of the flowfield during dynamic stall. Further qualitative descriptions of the dynamic stall phenomenon can be found in Refs. 6 and 7.

For repeated excursions into stall, considerable hysteresis in the force and moment behavior can arise and may lead to reduced or negative pitch damping. If stall becomes sufficiently severe on a rotor, this may excite the blade torsion mode at its natural frequency and can lead to a dynamic instability known as stall flutter. Thus, to define the rotor operating envelope, it is necessary to be able to predict this dynamic stall phenomenon and model its consequences on the performance and dynamic response of the rotor.

The unsteady aerodynamic response of an airfoil to a specific time history of forcing can now be determined with consid-

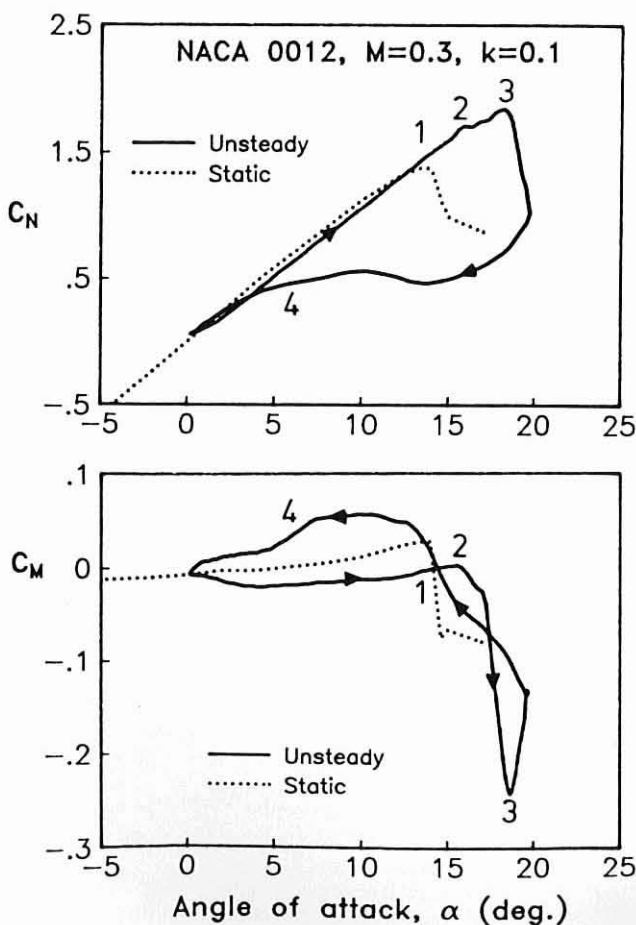


Fig. 1 Typical dynamic stall behavior of a NACA 0012 airfoil at $M = 0.3$. (Adapted from Ref. 6)

FLOW STRUCTURE	
1	FLOW REVERSALS WITHIN BOUNDARY LAYER, FORMATION OF VORTEX
2	VORTEX DETACHES AND MOVES OVER AIRFOIL SURFACE
3	VORTEX PASSES TRAILING EDGE, FULL STALL DEVELOPS
4	REATTACHMENT OF FLOW

FORCES AND MOMENTS	
1	EXCEEDS STATIC MAXIMUM LIFT, EXTRAPOLATE LINEAR RANGE
2	PITCHING MOMENT DIVERGENCE, VORTEX LIFT PRESENT
3	MAXIMUM LIFT, RAPID DECAY, MINIMUM PITCHING MOMENT, MAXIMUM DRAG
4	READJUST TO LINEAR RANGE

erable detail and accuracy using computational fluid dynamic (CFD) methods. For example, numerical solutions to the unsteady Navier-Stokes equations are now becoming increasingly feasible (Refs. 8 and 9) and have shown some recent success in modeling dynamic stall. Unfortunately, these aerodynamic solutions are extremely complex and the required computational resources are, for most routine rotor analyses, prohibitive. Nevertheless, CFD methods are providing considerable insight to the aerodynamic problems encountered by rotorcraft (Ref. 10) and ultimately will offer the most complete model of the flowfield. It appears, however, that for the foreseeable future more approximate aerodynamic solution methods must continue to be used in most rotor performance and aeroelasticity analyses. Clearly, this poses somewhat of a dilemma for the analyst as the consequences of complex viscous effects must be modeled within the practical constraints imposed by the computational enormity of overall rotor analysis.

To provide some representation of the unsteady aerodynamic behavior of the blade sections, a number of fairly sophisticated semi-empirically based models have been developed (e.g., Refs. 11–15). A good review of some of the capabilities of some other recent dynamic stall prediction methods is given in Ref. 16. Most of the semi-empirical models in use for helicopter rotor analyses have incompressible flow approximations for the unsteady aerodynamics under attached flow conditions and, for the dynamic stall regime, they often rely heavily on the synthesis of wind tunnel data from unsteady airfoil tests. In the interests of computational simplicity, some models sacrifice physical realism and so may have limited generality in application. Despite these limitations, developed methods have met with good success and have been shown to give significant improvements in performance prediction capability for helicopters. However, with the increasing operational demands that are placed on helicopters and the increasing use of advanced blade technology and modern airfoil sections, there is still a fundamental requirement for improved aerodynamic models that can be applied more generally and used with greater confidence in rotor design procedures.

It is the purpose of this paper to present the results of some research directed towards improving the representation of unsteady aerodynamics within a comprehensive rotor analysis. To this end, the effects of compressibility and dynamic stall are included. Furthermore, the method is presented in the time domain which is a necessary prerequisite to fully account for the flowfield encountered by a helicopter rotor. The main objective of the work is not simply to synthesize the unsteady airloads but to attempt to tackle the problem at a more physical level of approximation. As a consequence, it is necessary to model, in some approximate but physically representative way, the key features of the processes involved in the dynamic stall of an airfoil. It is shown in this paper that this approach can significantly reduce the very large number of parameters that are often inherent within some semi-empirical dynamic stall models. Numerical procedures are presented with the primary objective of providing a practical engineering method for incorporating the dynamic stall model in routine rotorcraft aerodynamics and aeroelastic response analyses.

Methodology

Attached Flow Behavior

A prerequisite to any unsteady aerodynamic model is the ability to model accurately the attached flow behavior. It is possible to formulate this problem in terms of a superposition of indicial aerodynamic responses. The derivation of the indicial lift and moment functions for compressible flows has been presented in numerous sources (e.g., Refs. 17–20). In the present analysis, the indicial response functions given by Beddoes (Ref. 21) and later refined by Leishman (Ref. 22) are used. These indicial responses are assumed to be composed of

the sum of two parts; one for the initial noncirculatory loading (which comes from piston theory, e.g. Ref. 19) and another for the circulatory loading which builds up quickly to the steady state value. The scaling normally adopted to nondimensionalize time produces the parameter $S = 2Vt/c$ which corresponds to the relative distance traveled by the airfoil in terms of semi-chords. For a step change in angle of attack, the normal force and pitching moment coefficients can be written in the S domain as

$$\Delta C_N(S) = \left[C_{N_a}(M) \phi_\alpha^C(S, M) + \frac{4}{M} \phi'_{\alpha_M}(S, M) \right] \Delta \alpha \quad (1)$$

$$\Delta C_M(S) = \left[\frac{-1}{M} \phi'_{\alpha_M}(S, M) + \left(\frac{1}{4} - x_{ac} \right) C_{N_a}(M) \phi_\alpha^C(S, M) \right] \Delta \alpha \quad (2)$$

The circulatory part of the indicial response, $\phi_\alpha^C(S, M)$, for a step change in angle of attack has been shown by Heaslet *et al.* (Ref. 18) to be similar to a Küssner type gust function. This indicial response can be approximated empirically in terms of the exponential function

$$\phi_\alpha^C(S, M) = 1.0 - A_1 \exp(-b_1 \beta^2 S) - A_2 \exp(-b_2 \beta^2 S) \quad (3)$$

where the constants are given by Beddoes (Ref. 21) as $A_1 = 0.3$, $A_2 = 0.7$, $b_1 = 0.14$, and $b_2 = 0.53$. It should be noted that the exponents are generalized to scale with β^2 to account for the effects of compressibility on the build-up of the circulatory loads. The noncirculatory indicial functions ϕ'_α and ϕ'_{α_M} are also approximately by exponential functions and can be generalized in terms of Mach number. A recent paper by Leishman (Ref. 22) discusses this approach in detail in which indicial moment responses and contributions due to pitch rate motion are also defined.

The above step response solutions can subsequently be manipulated by superposition using a finite-difference approximation to Duhamel's integral to construct the cumulative effect to an arbitrary time history of angle of attack. Development of the numerical algorithms to accomplish this were initially presented in Refs. 21 and 23. The basics of these procedures are recapitulated here in the light of recent enhancements to the representation of the indicial response functions over those given in Ref. 23.

The circulatory normal force due to an accumulating series of step inputs in angle of attack has been obtained using

$$C_{N_n}^C = C_{N_a}(M)(\alpha_n - X_n - Y_n) = C_{N_a}(M)\alpha_{E_n} \quad (4)$$

where n is the current sample. The deficiency functions are given by

$$X_n = X_{n-1} \exp(-b_1 \beta^2 \Delta S) + A_1 \Delta \alpha_n \exp(-b_1 \beta^2 \Delta S/2) \quad (5)$$

$$Y_n = Y_{n-1} \exp(-b_2 \beta^2 \Delta S) + A_2 \Delta \alpha_n \exp(-b_2 \beta^2 \Delta S/2) \quad (6)$$

where ΔS is the incremental distance traveled by the airfoil (in semi-chords) over the sample interval, $\Delta t = t_n - t_{n-1}$, and

$\Delta\alpha$ is the corresponding change in α from one time step to the next. The deficiency functions represent the "deficiency" in angle of attack due to unsteady aerodynamic effects and contain all the information about the time history of the shed wake effects on the airloads.

In a similar way, the noncirculatory normal force can be obtained from

$$C'_{N_n} = \frac{4K_\alpha T_I}{M} \left(\frac{\Delta\alpha_n}{\Delta t} - D_n \right) \quad (7)$$

where in this case the deficiency function is given by

$$D_n = D_{n-1} \exp\left(\frac{-\Delta t}{K_\alpha T_I}\right) + \left(\frac{\Delta\alpha_n - \Delta\alpha_{n-1}}{\Delta t} \right) \exp\left(\frac{-\Delta t}{2K_\alpha T_I}\right) \quad (8)$$

The deficiency function in Eq. 8 essentially accounts for time-history effects on the airloads due to the accumulation of wave-like pressure disturbances. The noncirculatory time constant governing the decay of the loads due to the propagation of pressure disturbances is given by $T_I = c/a$, which is a result given previously in Ref. 23. The factor K_α , which is associated with the noncirculatory time constant, is a function of Mach number

$$K_\alpha = \frac{0.75}{(1 - M) + \pi\beta^2 M^2 (A_1 b_1 + A_2 b_2)} \quad (9)$$

and is derived using the exact linear theory of Lomax (Ref. 17). For $M \rightarrow 0$, $K_\alpha \rightarrow 0.75$, which is the value used previously in Ref. 23. The evaluation of all the noncirculatory time constants is discussed in detail in Ref. 22.

The total normal force coefficient under attached flow conditions, C'_N , is given by the sum of circulatory and noncirculatory components

$$C'_N = C'_{N_n} + C'_{C_n} \quad (10)$$

The numerical procedures for the evaluation of pitch rate and pitching moment terms can be evaluated in an identical way using the indicial response functions of Ref. 22.

The unsteady chord (in-plane) force coefficient, C_C , may be obtained using the effective angle of attack α_E

$$C_C = C_{N_n} \tan \alpha_E \approx C_{N_n}(M) \alpha_E^2 \quad (11)$$

Subsequently, the unsteady pressure drag is obtained by resolving the total normal force and chord force coefficients through the pitch angle to obtain

$$C_D = C_{N_n} \sin \alpha_n - C_C \cos \alpha_n \quad (12)$$

It should be noted that, under unsteady (potential flow) conditions, the instantaneous pressure drag may actually become negative. Further details on modeling the unsteady chord force and pressure drag are given in Refs. 23 and 24.

Leading Edge Separation

The most critical aspect of modeling dynamic stall is to define the conditions under which leading edge separation occurs. Because of its importance to the dynamic stall problem, this will be discussed first.

Evans and Mort (Ref. 25) present a useful criterion equivalent to a critical leading edge pressure and associated pressure

gradient which may be used to denote the onset of static leading-edge stall. This criterion was subsequently evaluated by Beddoes (Ref. 26) within the context of rotor airfoil performance, under both steady and unsteady conditions. For practical purposes, Beddoes determined that, although under time-dependent forcing conditions the pressure gradient on the airfoil at a given angle of attack was significantly modified, it was possible to predict the onset of leading edge separation (and hence, dynamic stall) using a criterion in which the attainment of a critical local leading-edge velocity (pressure) was the primary factor. The analysis was subsequently extended by Beddoes (Ref. 27) to encompass higher Mach number flows, where the attainment of a critical leading edge pressure corresponding to shock reversal was used to denote the onset of shock induced stall.

In application, the leading edge pressures are related to the normal force, C_N , so it is possible to obviate the need to compute airfoil pressures by transforming the calculation to the C_N domain. From an analysis of airfoil static test data, a critical value of $C_N(\text{static}) = C_{N_c}$ may be obtained which corresponds to the critical pressure for separation onset at the appropriate Mach number. Thus, a Mach number dependent, separation onset (stall) boundary may be defined. A typical boundary for the NACA 0012 airfoil is shown in Fig. 2. Boundaries for other airfoils may be derived accordingly if the static chordwise pressure distributions are known. In practice, however, C_{N_c} can be obtained from the value of $C_N(\text{static})$ that corresponds to either the break in the pitching moment or the chord force at stall.

For unsteady conditions, there is a lag in $C_N(t)$ with respect to changes in angle of attack; however, there is also a lag in the leading edge pressure response with respect to $C_N(t)$. Thus, for an increasing angle of attack, the lag in the leading edge pressure response results in the critical pressure being achieved at a higher value of C_N , and hence, at a higher angle of attack than for the quasi-steady case. Thus, this mechanism significantly contributes to the overall delay in the onset of dynamic stall. To implement the critical pressure criterion under unsteady conditions, a first-order lag may be applied to $C_N(t)$ to produce a substitute value $C'_N(t)$ with the presumption that whatever properties apply to the pressure must also apply to $C'_N(t)$. For a discretely sampled system, this compensation to $C_N(t)$ may be written in numerical form as

$$C'_{N_n} = C_{N_n} - D_{p_n} \quad (13)$$

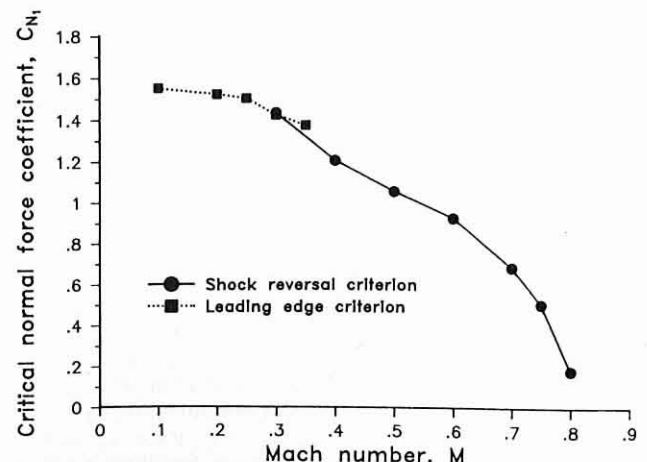


Fig. 2 Critical normal force separation onset boundary for the NACA 0012 airfoil.

where the deficiency function is given by

$$D_{p_n} = D_{p_{n-1}} \exp\left(\frac{\Delta S}{T_p}\right) + (C_{N_n}^p - C_{N_{n-1}}^p) \exp\left(\frac{\Delta S}{2T_p}\right) \quad (14)$$

The results of this compensation procedure are shown in Fig. 3 where the leading edge pressure coefficient at 1 percent chord for a harmonic pitch oscillation is plotted versus the corresponding $C_N(t)$ and $C'_N(t)$. It can be seen that, for different reduced frequencies, when pressure is plotted versus $C'_N(t)$ using a suitable value of T_p , the curves collapse to a single line which in fact represents the static relation. Thus, in terms of the value of $C'_N(t)$, the onset of leading edge/shock induced separation under dynamic conditions will be initiated when $C'_N(t)$ exceeds the critical $C_{N_1}(M)$ boundary. This means that there will be a delay in the onset of leading edge separation to higher angles of attack for increasing reduced frequency (or increasing pitch rate). Furthermore, if the value of $C'_N(t)$ is monitored throughout the calculation into stall, then it may be used as an indicator for the conditions which permit flow reattachment (i.e., if $C'_N(t) < C_{N_1}$).

It should be noted that the time constant T_p is a function of Mach number and must be determined empirically from unsteady airfoil data. (Appropriate values are given for the NACA 0012 airfoil in Ref. 23.) However, it appears that the values of T_p are largely independent of airfoil shape. Such a conclusion may be drawn by performing a similar analysis on unsteady data obtained by McCroskey (Ref. 28) for various airfoils, albeit over a limited range of Mach numbers.

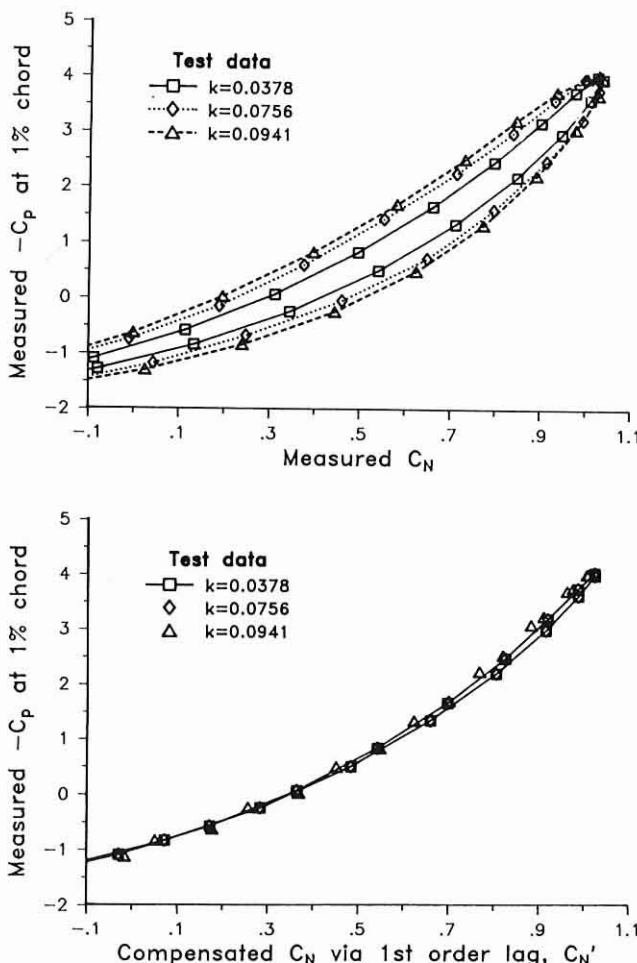


Fig. 3 Compensation of unsteady leading edge pressures for the NACA 0012 at $M = 0.4$.

Trailing Edge Separation

Before discussing the subsequent airloads induced after the initiation of dynamic stall, it is necessary to discuss another mechanism that is also involved in most types of airfoil stall. This is progressive trailing edge separation. The associated loss of circulation due to trailing edge separation introduces a nonlinear force and moment behavior, especially with the cambered airfoils more typically used on modern helicopters. Wilby (Ref. 29) suggests that trailing edge separation may play a significant role in the onset of dynamic stall. However, as also discussed by Wilby, experimental tests have indicated that the occurrence of trailing edge separation is suppressed by increasing pitch rate. The dynamic stall process may then be initiated by leading-edge separation or shock induced separation if supercritical flow is allowed to develop. Even so, when the primary source of separation is either at the leading edge or at the foot of a shock wave, it appears that this is generally sufficient to promote some separation at the trailing edge and hence initiate some nonlinear behavior in the force and moment response.

One theory which models separated flow regions on 2-D bodies is attributed to Kirchhoff and is reviewed in Refs. 30 and 31. A specific case of Kirchhoff flow is a simple model for the trailing edge separation phenomenon in which the airfoil normal force coefficient, C_N , may be approximated as

$$C_N = 2\pi \left(\frac{1 + \sqrt{f}}{2} \right)^2 \alpha \quad (15)$$

where 2π is the force-curve-slope for incompressible flow, f is the trailing edge separation point and α is the angle of attack. Thus, if the separation point can be determined, it is a trivial calculation to determine the normal force. In practical cases, this expression may be extended to encompass compressible flows where 2π is replaced by the force-curve-slope at the appropriate Mach number

$$C_N = C_{N_a}(M) \left(\frac{1 + \sqrt{f}}{2} \right)^2 \alpha \quad (16)$$

To implement this procedure, the relationship between the effective separation point, f , and the angle of attack, α , can be deduced from the airfoil static C_N behavior by rearrangement of Eq. 16 to solve directly for f . The relationship between α and f can be generalized empirically in a fairly simple manner using the relations

$$f = \begin{cases} 1 - 0.3 \exp\{(\alpha - \alpha_1)/S_1\} & \text{if } \alpha \leq \alpha_1 \\ 0.04 + 0.66 \exp\{(\alpha_1 - \alpha)/S_2\} & \text{if } \alpha > \alpha_1 \end{cases} \quad (17)$$

The coefficients S_1 and S_2 define the static stall characteristic, while α_1 defines the break point corresponding to $f = 0.7$. It should be noted that $f \approx 0.7$ closely corresponds to the static stall angle of attack for most airfoil sections. S_1 , S_2 , and α_1 are easily determined for different Mach numbers from the static lift data.

A general expression for the pitching moment behavior cannot be obtained from Kirchhoff theory, and an alternative empirical relation must be formulated. From the airfoil static data, the center of pressure at any angle of attack may be determined from the ratio C_M/C_N (allowing for the zero lift moment C_{M_0}). The variation can be plotted versus the corresponding value of the separation point and curve fitted using a suitable polynomial. One suitable fit is to use the form

$$\frac{C_M}{C_N} = K_0 + K_1(1 - f) + K_2 \sin(\pi f^m) \quad (18)$$

where $K_0 = (0.25 - x_{ac})$ is the aerodynamic center offset from the 1/4-chord. The constant K_1 gives the direct effect on the center of pressure due to the growth of the separated flow region and the constant K_2 helps describe the shape of the moment break at stall. The values of K_0 , K_1 , K_2 and m can be adjusted for different airfoils, as necessary, to give the best moment reconstruction. For the NACA 0012 a value of $m = 2$ has been used; however values of $m = 1/2$ or $m = 1$ can be used as necessary for other airfoils to obtain the best fit with the test data.

Using the above equations, the reconstructed static lift and moment versus angle of attack relationships are shown for the NACA 0012 airfoil at Mach numbers of 0.3, 0.5, and 0.7 in Fig. 4. This procedure has also been validated for other airfoils, and can be applied to almost any airfoil if the static stall characteristics are known *a priori*.

An expression for the chord force C_C may also be deduced from the Kirchhoff solution to the trailing edge stall problem

$$C_C^f = \eta C_{N_a} \alpha^2 \sqrt{f} \quad (19)$$

where the factor \sqrt{f} accounts for the influence of trailing edge separation. Even with no separation on the airfoil, the airfoil does not realize 100 percent of the chord force which would be attained in potential flow. Allowance for this nonrealization is made through the recovery factor η which can be obtained empirically from static airfoil test data. Typically, $\eta \approx 0.95$. The pressure drag in separated flow can be obtained through resolution of the chord force and normal force through the pitch angle as in Eq. 12. The total section drag is obtained by addition of the viscous drag component C_D . Note that for

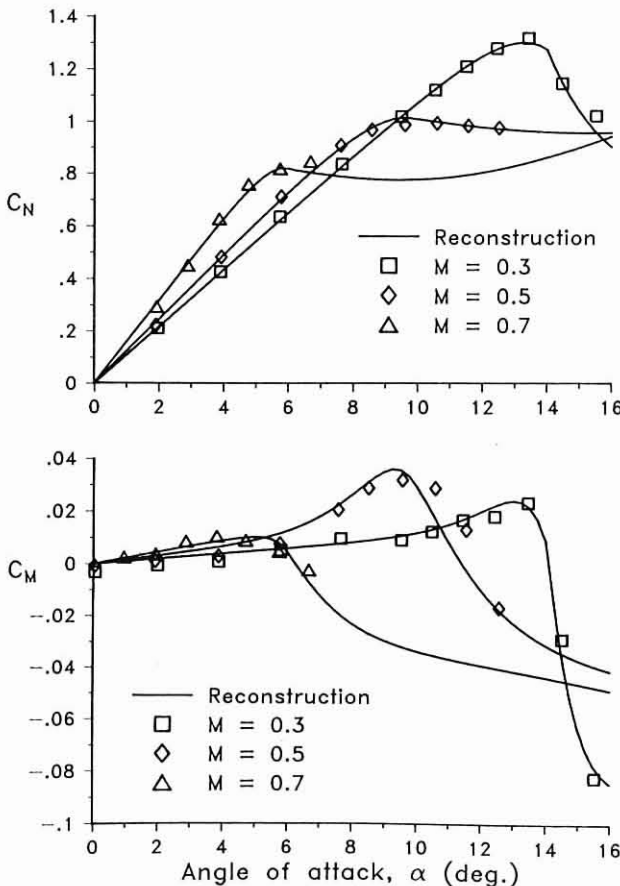


Fig. 4 Reconstruction of static normal force and pitching moment behavior for the NACA 0012 at various Mach numbers.

inviscid flow, $C_D = 0$, $\eta = 1$ and $f = 1$; so, for steady conditions, Eq. 12 reduces to the classical result that $C_D = 0$.

For unsteady flow, there exists a modified separation point location due to the temporal effects on the airfoil pressure distribution and the boundary layer response. An open loop procedure has been developed to represent these effects on the trailing edge separation point and thereby permit the evaluation of nonlinear forces and moments under dynamic conditions via the application of the Kirchhoff theory, as above.

The procedure is performed by firstly incorporating the airfoil unsteady pressure response via Eqs. 13 and 14. This may then be used to define an effective angle of attack, α_f , which gives the same unsteady leading edge pressure as for the equivalent quasi-steady case

$$\alpha_f(t) = \frac{C'_N(t)}{C'_{N_a}(M)} \quad (20)$$

This value of α_f may be used to determine a value for the effective separation point f' at this α_f from the static f versus α relationship in Eq. 17. Secondly, the additional effects of the unsteady boundary layer response may be represented by application of a first-order lag to the value of f' to produce the final value for the unsteady trailing edge separation point f'' . For a discretely sampled system, this may be represented in numerical form as

$$f''_n = f'_n - D_{f_n} \quad (21)$$

where the deficiency function is

$$D_{f_n} = D_{f_{n-1}} \exp\left(\frac{\Delta S}{T_f}\right) + (f'_n - f'_{n-1}) \exp\left(\frac{\Delta S}{2T_f}\right) \quad (22)$$

As in the case of T_p , T_f is a Mach number dependent time constant (see Ref. 23), albeit a much weaker variation than with T_p . However, it is more difficult to define how this time constant will change with airfoil shape. Without access to unsteady airfoil data, an unsteady boundary layer code along the lines of Ref. 32 can be practically used to determine how T_f varies with airfoil shape (see also Ref. 27 for discussion).

Finally, the (nonlinear) normal force C_N^f incorporating the effects of the modified (unsteady) trailing edge separation point f'' is given by the Kirchhoff relation

$$C_N^f = C_{N_a}(M) \left(\frac{1 + \sqrt{f''_n}}{2} \right)^2 \alpha_{E_n} + C_{N_0}^f \quad (23)$$

and the pitching moment by

$$C_M^f = [K_0 + K_1(1 - f''_n) + K_2 \sin(\pi(f''_n)^m)] C_N^f + C_{M_0} \quad (24)$$

where C_N^f is the circulatory normal force coefficient and C_{M_0} is the zero-lift moment. The contributions of the other unsteady circulatory and noncirculatory moment terms are additive to Eq. 24. Similarly, the chord force is given as

$$C_C^f = \eta C_{N_a} \alpha_{E_n}^2 \sqrt{f''_n} \quad (25)$$

Dynamic Stall

The general case of dynamic stall involves the formation of a vortex near the leading edge of the airfoil which subsequently separates from the surface and is transported downstream. It appears that, until the vortex begins to detach, there are no gross changes in the airfoil pressure distribution, and the forces

and moments can be represented as if the developing vortex is ignored. After the vortex detaches, the stall development appears to be governed by a basic common process; qualitatively similar effects have been obtained for different modes of forcing such as oscillatory pitch, plunge, and ramp motions (e.g., Refs. 29 and 33).

A physically acceptable model for the vortex induced lift has been formulated by viewing the vortex lift contribution as an excess accumulation of circulation that is retained in the vicinity of the airfoil until some critical condition is reached. For a discretely sampled system, the vortex lift force coefficient $C_{N_n}^v$ is represented by assuming that, for a given sample period, the increment in vortex lift C_v is determined by the difference between the instantaneous linearized value of the unsteady circulatory lift and the corresponding unsteady nonlinear lift as given by the Kirchhoff approximation, i.e.

$$C_{v_n} = C_{N_n}^v (1 - K_{N_n}) \quad (26)$$

where

$$K_{N_n} = (1 + \sqrt{f''_n})^2/4 \quad (27)$$

At the same time, the total accumulated vortex lift C_N^v is allowed to decay exponentially with time, but may also be updated by a new increment. Following the approach used above, this process may be written in discrete time form as

$$C_{N_n}^v = C_{N_{n-1}}^v \exp\left(\frac{\Delta S}{T_v}\right) + (C_{v_n} - C_{v_{n-1}}) \exp\left(\frac{\Delta S}{2T_v}\right) \quad (28)$$

Consequently, when the rate of change of lift is low, the vortex lift is being dissipated as fast as it accumulates; in the limit as the rate of change tends to zero, the airfoil characteristics revert smoothly back to the static (nonlinear) behavior.

Abrupt airloading changes occur when the critical conditions for leading edge or shock induced separation effects are met (i.e., $C_N^v(t)$ exceeds the $C_{N_1}^v$ /Mach number boundary). At this point, the accumulated vortex lift is assumed to start to convect over the airfoil chord. The rate at which this convection process occurs has been determined from experimental tests to be somewhat less than half of the free-stream velocity, with a weak dependence on Mach number. During the vortex convection process, the vortex lift is assumed to continue via Eqs. 26–28 but the accumulation is terminated when the vortex reaches the airfoil trailing edge and is shed into the wake. To track the position of the vortex, a nondimensional vortex time parameter τ_v (in semi-chords) is used such that $\tau_v = 0$ at the onset of separation conditions and $\tau_v = T_{vl}$ when the vortex reaches the trailing edge.

The center of pressure on the airfoil also varies with the chordwise position of the vortex and will obtain a maximum value when the vortex reaches the trailing edge. Based on an analysis of much experimental data involving dynamic stall over a wide range in Mach number, a fairly general representation of the center of pressure behavior (aft of 1/4-chord) was formulated empirically as

$$CP_v = 0.20 \left(1 - \cos\left(\frac{\pi\tau_v}{T_{vl}}\right)\right) \quad (29)$$

Finally, the increment in pitching moment about the quarter-chord due to the aft-moving center of pressure is given by

$$C_M^v = -CP_v C_N^v \quad (30)$$

Both the vortex decay time constant T_v and the nondimensional time for the vortex to traverse the chord T_{vl} were also

determined empirically from unsteady test data, and values are presented for the NACA 0012 in Ref. 23. Both T_v and T_{vl} appear relatively independent of Mach number over most of the Mach number range. However, no formal conclusion can be made here regarding the variability of these parameters with airfoil shape. The dynamic stall experiments performed by McCroskey *et al.* (Refs. 28 and 34) indicate that, while there is a significant effect of airfoil shape under light stall conditions, all airfoils behave very similarly under strong dynamic stall conditions. Thus, it can be tentatively concluded that the parameters T_v and T_{vl} should be relatively insensitive to airfoil shape.

From the above, the required total loadings can be obtained by superposition. For example, the total normal force coefficient C_N under dynamic stall conditions is given by

$$C_N(t) = C_N^v(t) + C_N^s(t) \quad (31)$$

with a similar equation for the pitching moment.

Indications of multiple vortex shedding phenomena during dynamic stall were apparent in many of the ramp and oscillatory pitch test data, especially in the higher incidence range and at lower reduced frequencies and pitch rates. This was manifested by multiple peaks in the normal force, drag, and pitching moment response for which the secondary peak was generally of most significance. In the high incidence range, the frequency of vortex shedding was determined to correspond closely to a Strouhal number $St = 0.19$, which appeared relatively independent of Mach number. A simple model for the process was developed by allowing secondary increments in vortex lift to build up again via Eqs. 26–28 after a nondimensional time T_{St} (instead of T_{vl}) corresponding to an effective flat plate Strouhal number based on the position of the trailing edge separation point, i.e.

$$T_{St} = \frac{2(1 - f'')}{St} \quad (32)$$

Using this simple model, the force and moment characteristics of multiple vortex shedding were found to be reasonably well represented during both the ramp and oscillatory pitch tests (see results below).

Modifications to the Model

Although the above system equations describe, in an open loop sense, the basic physical flow phenomena likely to be encountered on most airfoils, the elements of the model are, in fact, physically coupled. For example, trailing edge separation development will be curtailed with the onset of leading edge separation. Also, the initiation of flow reattachment will be delayed if the airfoil is undergoing leading edge vortex shedding, even though the angle of attack may be low enough to initiate flow reattachment under normal conditions. As shown in Ref. 23, the coupling of the elements of the nonlinear model can be readily represented by a temporary modification to the appropriate time constant associated with the behavior (i.e., by a simple halving or doubling of the time constant associated with one process during some critical phase of another process). For example, airfoil test data indicate that leading edge or shock induced separation may occur very abruptly. To implement these phenomena via the critical leading edge pressure criterion, it is sufficient to over-ride the lag associated with trailing edge separation by halving the T_f time constant. To maximize generality for other airfoil sections, these modifications were restricted to the two time constants T_f and T_v only.

While modifying the time constants may not be particularly desirable, this does avoid coupling the flow elements of the model using the addition of further equations and possibly the use of more time constants. It should be noted, however, even

if the modifications to the time constants T_f and T_v are not implemented, the basic elements of the model are still sufficient to produce accurate predictions of the force and moment characteristics of dynamic stall. The various strategies to modify the time constant have been developed using experimental data as a guide and by correlating the model with some 200 test cases of dynamic stall over a range of Mach numbers from 0.3 to 0.8. These strategies are detailed in Ref. 23 and involve minimal additional logic in the overall algorithm. It should be noted that modifications to the time constants are intended to be fixed features of the model.

Other minor modifications have been made to the model based on experience in correlating with a large amount of experimental data for dynamic stall. These included modifications to the chord force calculation under deep stall conditions and the modeling of the center of pressure during flow reattachment from dynamic stall. Again, all the details of these modifications are discussed in Ref. 23.

Results and Discussion

This section documents a selection of comparisons of the aerodynamic model with unsteady test data. The bulk of the data presented are for a NACA 0012 airfoil and were obtained in a blow-down wind tunnel at the Aircraft Research Association (A.R.A.) in the U.K. The tunnel has a test section which is 45cm in height and 20cm wide with slotted upper and lower walls. The airfoil model, which spanned the width of the tunnel, had a chord of 10cm. Surface pressures were measured using miniature pressure transducers distributed at 30 positions around the chord at mid-span. Forces and moments were obtained from the integration of pressures. The wind-tunnel was pressurized

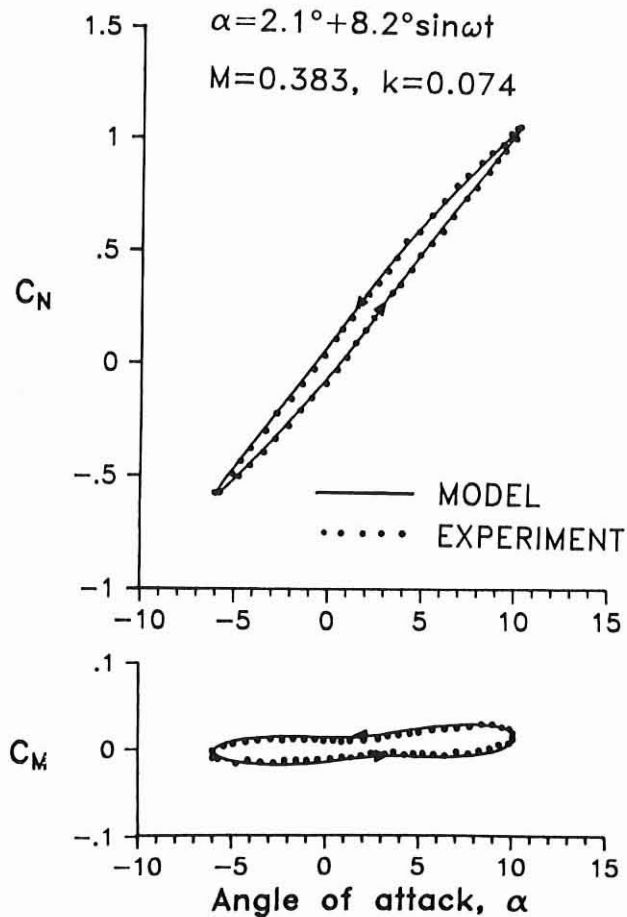


Fig. 5 Prediction of normal force and pitching moment under attached flow conditions at $M = 0.4$.

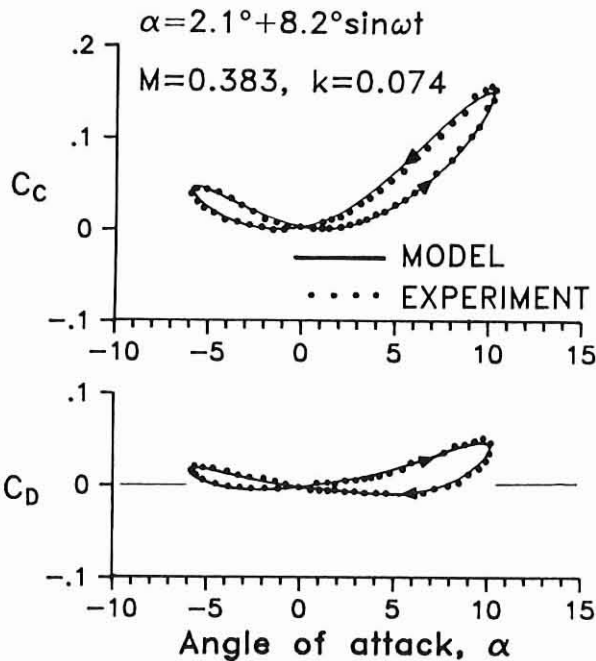


Fig. 6 Prediction of chord force and pressure drag under attached flow conditions at $M = 0.4$.

to give a Reynolds number of approximately $Re = M \times 10^7$ which is close to full scale helicopter rotor values. Both oscillatory pitch and constant pitch rate (ramp) tests were conducted. For the purposes of comparing the model with test data, the time history of the angle of attack forcing as measured in the experiment was used directly as an input to the model.

Typical normal force and pitching moment responses are shown in Fig. 5 for a harmonic pitch oscillation at a nominal reduced frequency of 0.075 and $M = 0.4$ under attached flow conditions. It should be noted that, for a pure sinusoidal oscillation under attached flow conditions, nominally elliptical

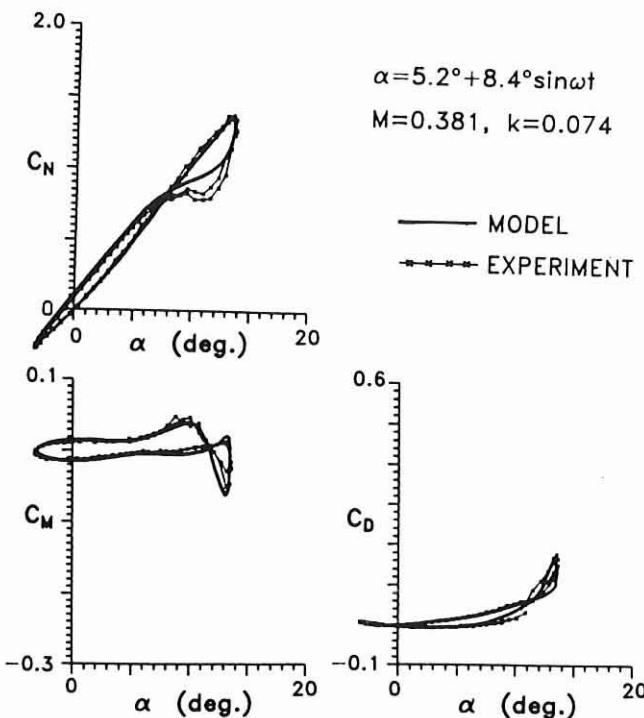
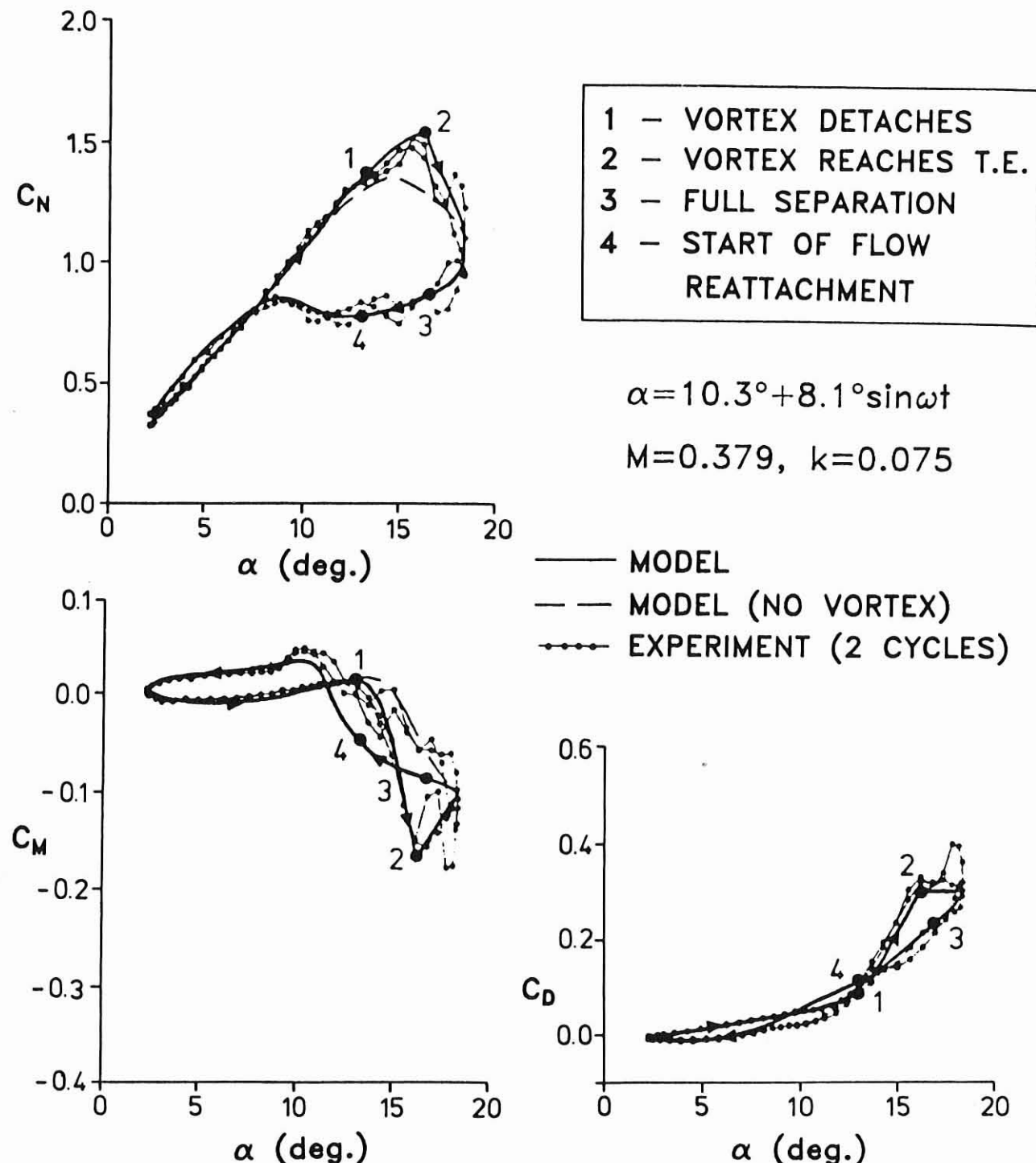


Fig. 7 Prediction of forces and moments during light dynamic stall at $M = 0.4$.

Fig. 8 Prediction of forces and moments during strong dynamic stall at $M = 0.4$.

lift and moment loops should be obtained. However, it can be seen that there is some distortion in the loops, particularly for the pitching moment. This behavior was traced to a significant third harmonic in the pitch forcing that has the effect of increasing the pitch rate contributions to the airloads near the maximum and minimum angles of attack. In Fig. 6, the corresponding predictions of the chord force and pressure drag are shown. It is worth noting the behavior of the unsteady pressure drag, which clearly shows that the drag becomes negative (i.e., a propulsive force) on the downstroke of the motion. The excellent correlations obtained for all components of the loading give considerable confidence in the ability to model the attached flow behavior.

In Fig. 7, the mean angle of attack is increased to 5.2° which is a typical case of light dynamic stall penetration (i.e., the maximum angle of attack is just sufficient to cause leading edge separation). It can be seen that all three components of the loading show deviations from the attached flow behavior near the maximum angles of attack because of the development of limited flow separation. As the angle of attack is reduced, the flow quickly reattaches. Although it was found that light dynamic stall was quite difficult to model, the predictions were in good agreement with the test data. The pitch damping for this case is quite low and indicates that the stall onset conditions may be conducive to stall flutter.

In Fig. 8, the mean angle of attack is increased such that

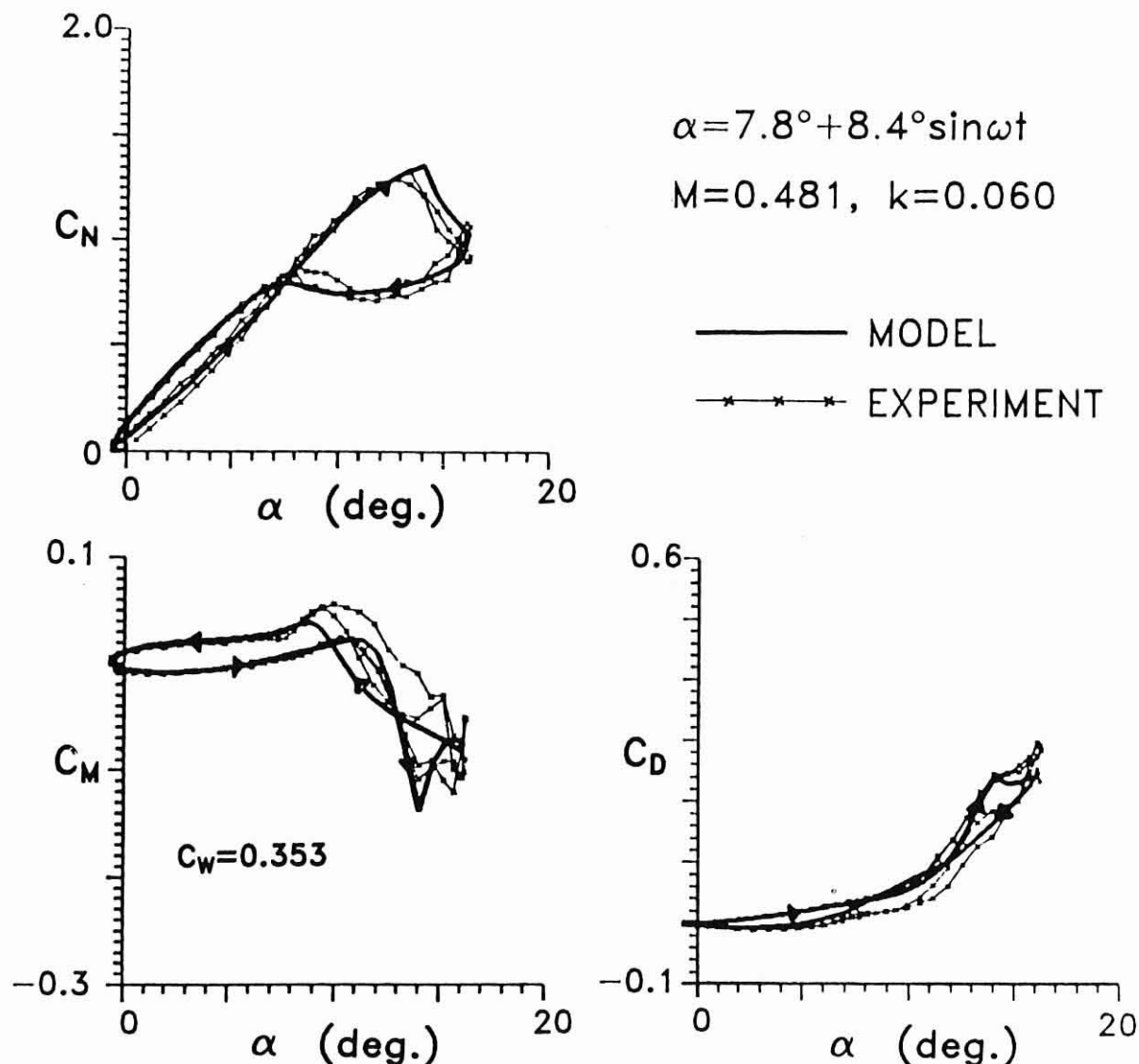
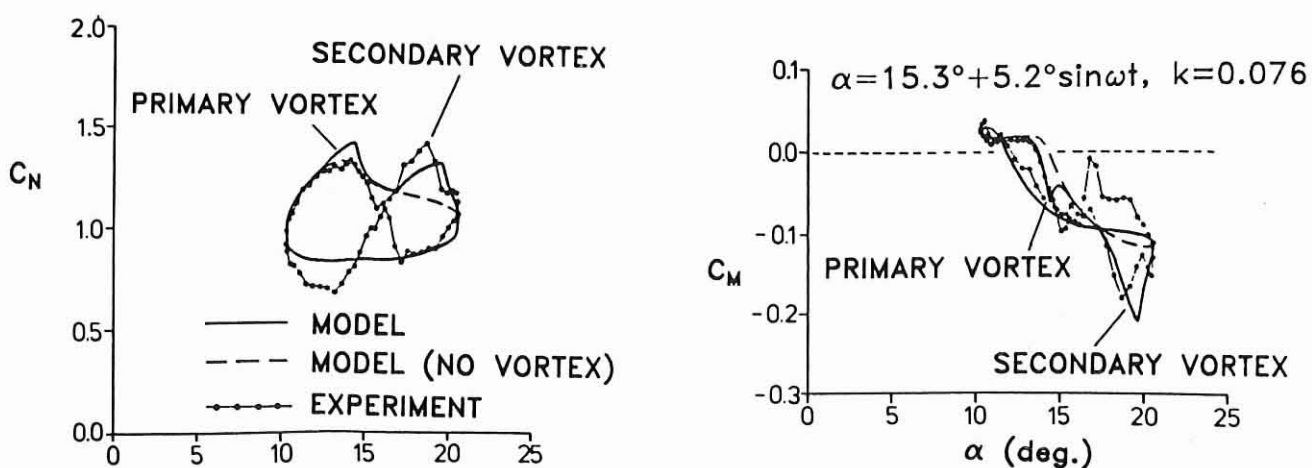
Fig. 9 Prediction of forces and moments during strong dynamic stall at $M = 0.5$.

Fig. 10 Prediction of secondary vortex shedding during dynamic stall.

strong dynamic stall occurs. (The same reduced frequency of 0.075 is maintained, as in the previous cases.) The modeling is shown with and without the contribution from the vortex lift. It can be seen that the vortex shedding contributes a moderate increment to $C_{N_{MAX}}$, but gives a particularly large increase in nose-down pitching moment. The maximum lift and minimum moments are predicted very accurately along with the phasing of the loads during stall. Flow reattachment (indicated by the return to the nominally elliptical shapes of the loops) is delayed to a fairly low angle of attack during the downstroke of the motion. It should be noted that two successive cycles of oscillatory pitch data are shown, and this serves to illustrate the inherent variability of the aerodynamic loads in the separated flow regime.

Another case of strong dynamic stall is shown in Fig. 9 and should be examined in conjunction with Fig. 8. This figure illustrates the basic similarity of the effects of dynamic stall at a higher Mach number of 0.5, but adjusted to a lower mean angle of attack datum.

In Fig. 10, the mean angle of attack is increased further, but the oscillation amplitude is reduced to 5° , still at a reduced frequency of 0.075. Under these conditions, strong secondary vortex shedding occurs which, in fact, is responsible for the maximum loads on the airfoil. It can be seen that the model captures this secondary vortex shedding phenomenon quite well. Some evidence of tertiary vortex shedding is also indicated on the downstroke of the airfoil motion, but no attempt was made to model this phenomenon here.

Figure 11 shows the effect of ramp pitch rate on the airfoil normal force, moment, and drag response. It is worth noting the delay of the separation onset conditions with increasing pitch rate, the overall increase in maximum lift, and the distinct periodicity of the airloads in the post stall regime. This figure also indicates the effectiveness of the leading edge separation criterion in predicting the delay and final onset of dynamic stall for widely different pitch rates. For the modeling, the multiple vortex shedding option gives a reasonable correlation with the test data in the post stall regime.

Figure 12 illustrates the effect of Mach number on the dynamic stall development (drag not shown). In this figure, the Mach number is increased from 0.488 to 0.692 but under the same nominal forcing conditions and at approximately the same reduced frequency. Of particular note here are the increasing amounts of hysteresis in the force and moment as the Mach number is increased. This occurs because, at a constant reduced frequency, the angle of attack for the onset of leading edge separation will decrease with increasing Mach number. In all three cases, the predictions of the model are in good agreement with the test data showing that the effects of Mach number on dynamic stall are well represented.

Figure 13 shows that, by increasing the reduced frequency for the same nominal angle of attack forcing (c.f. $M = 0.488$ case in Fig. 12), the amount of flow separation can be suppressed. While nominally elliptical loops are obtained at these conditions, the loss of lift during the reattachment process indicates that the amount of trailing edge separation is still sufficient to affect the airloads. Again, the behavior predicted by the model is in good agreement with the test data and proves that the effects of frequency in terms of suppressing separation development are adequately represented.

While the previous cases have referred specifically to modeling of the NACA 0012 airfoil characteristics, the ultimate proof of any aerodynamic model is the ability to predict the dynamic stall characteristics of an arbitrary airfoil. While an extensive correlation study with other airfoil sections is beyond the scope of the present paper, it is sufficient to demonstrate here computed predictions for two representative modern rotor airfoils, namely a Hughes HH-02 and a Sikorsky SC-1095 airfoil. The test data have been taken from those recorded in Ref. 28 and are for a Mach number of 0.3.

Of the various empirical constants that are used for the model, all but four of the parameters are derived from the static airfoil characteristics. The necessary static parameters for the HH-02 and the SC-1095 have been derived for the model using exactly the same procedure as for the NACA 0012 discussed previously. The dynamic time constants T_p , T_f , T_v and T_{vt} were retained from the values used for the NACA 0012 at the same Mach number.

Predictions of the lift and moment response are shown with the test data in Fig. 14 for a case of strong dynamic stall. The results are in remarkably good agreement with the test data and demonstrate the ability of the present model to predict, at least to an engineering level of approximation, the dynamic stall characteristics of other airfoil sections given the static stall behavior. The results also tend to support the previously made hypothesis that the dynamic time constants are relatively insensitive to airfoil shape. However, the validity of this latter statement can only be confirmed when unsteady airfoil data become available for higher Mach numbers.

Conclusions

1. The objective behind the work outlined in this paper has been to develop an improved semi-empirical model for the effects of dynamic stall. The approach adopted has been to tackle the problem at a more physical level of approximation, but still in a sufficiently simple manner and computational form to include it within a comprehensive rotor performance or aeroelasticity analysis. The ultimate objective of this line of approach is directed towards the development of a more general engineering model for the effects of dynamic stall that can be applied to a variety of conventional and advanced airfoils used for new rotor designs.

2. An indicial response and superposition method has been selected for the attached flow aerodynamics along with compressibility corrections in order to accurately capture both amplitude and phasing of the unsteady aerodynamic response. The nonlinear effects of trailing edge separation have been implemented under time-dependent conditions using the Kirchhoff theory as a means of relating the force and moment characteristics to the location and progression of the trailing edge separation point. Features of leading edge or shock induced separation have been reviewed and are implemented via a critical normal force coefficient/Mach number boundary. This procedure has been extended to the dynamic regime to denote the initiation of dynamic stall. Finally, the induced lift and pitching moment behavior during dynamic stall have been represented in a physically realistic manner. All the above phenomena are modeled in a manner that can be readily integrated into a subroutine for the blade sectional aerodynamics.

3. An extensive validation of the model has been conducted with unsteady test data for NACA 0012 undergoing both oscillatory pitch and ramp changes in angle of attack. Correlation with the test data was good, particularly in terms of predicting the onset of dynamic stall. The subsequent magnitude phasing of the dynamic stall loads for variations in both Mach number and reduced frequency was also in good agreement with the test data.

4. A brief validation has also been shown for the HH-02 and SC-1095 airfoil sections using only changes to the parameters of the model that can be derived directly from the static airfoil characteristics. The predictions for these airfoils are also in good agreement with the test data, and it appears the model may be sufficiently general to allow its application to other airfoil sections, at least when engineering levels of prediction capability are required. The level of correlation obtained with this new unsteady aerodynamic model provides considerable confidence when applied in the design of new rotors.

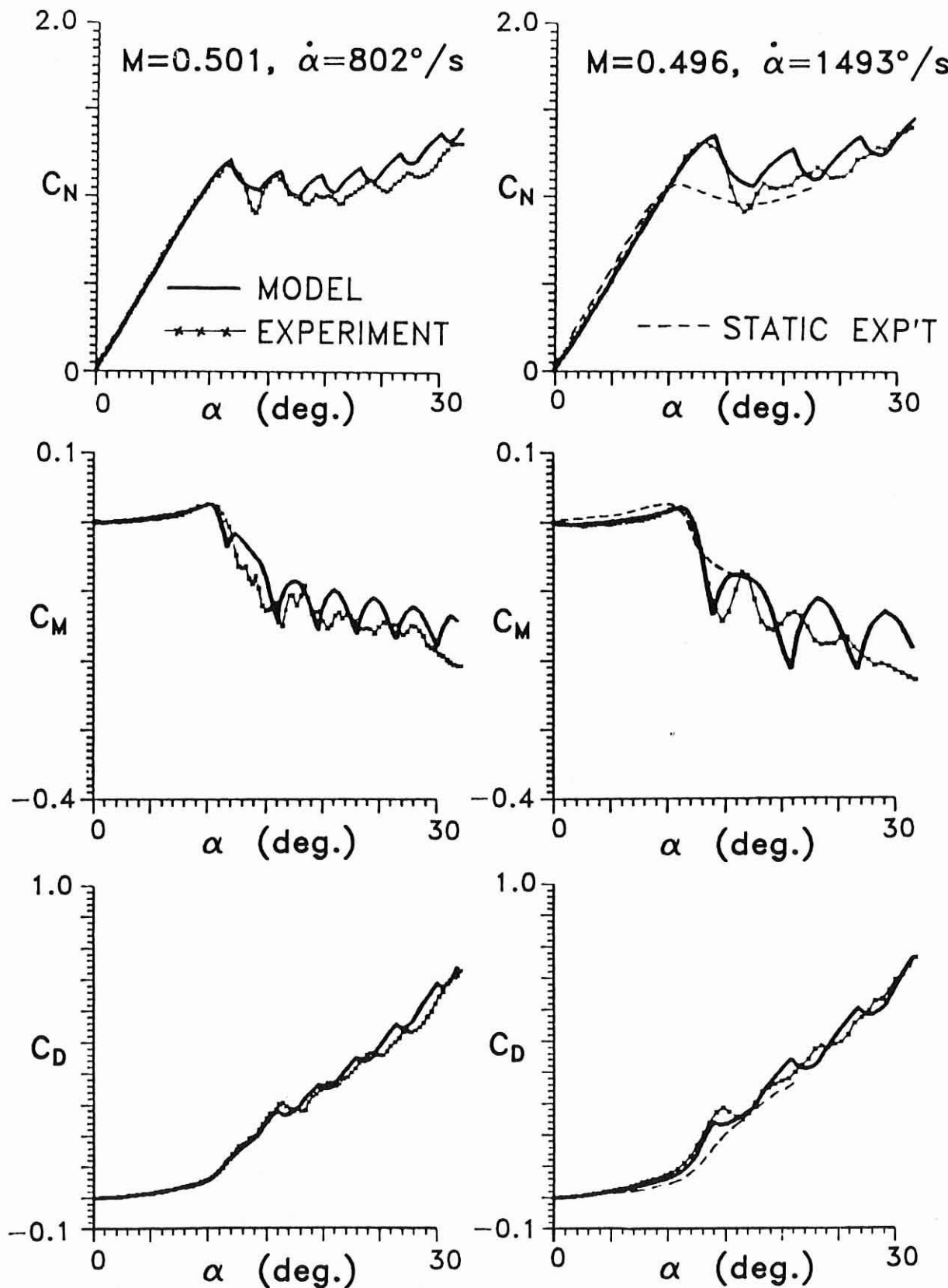


Fig. 11 Effects of ramp pitch rate on normal force, pitching moment, and pressure drag.

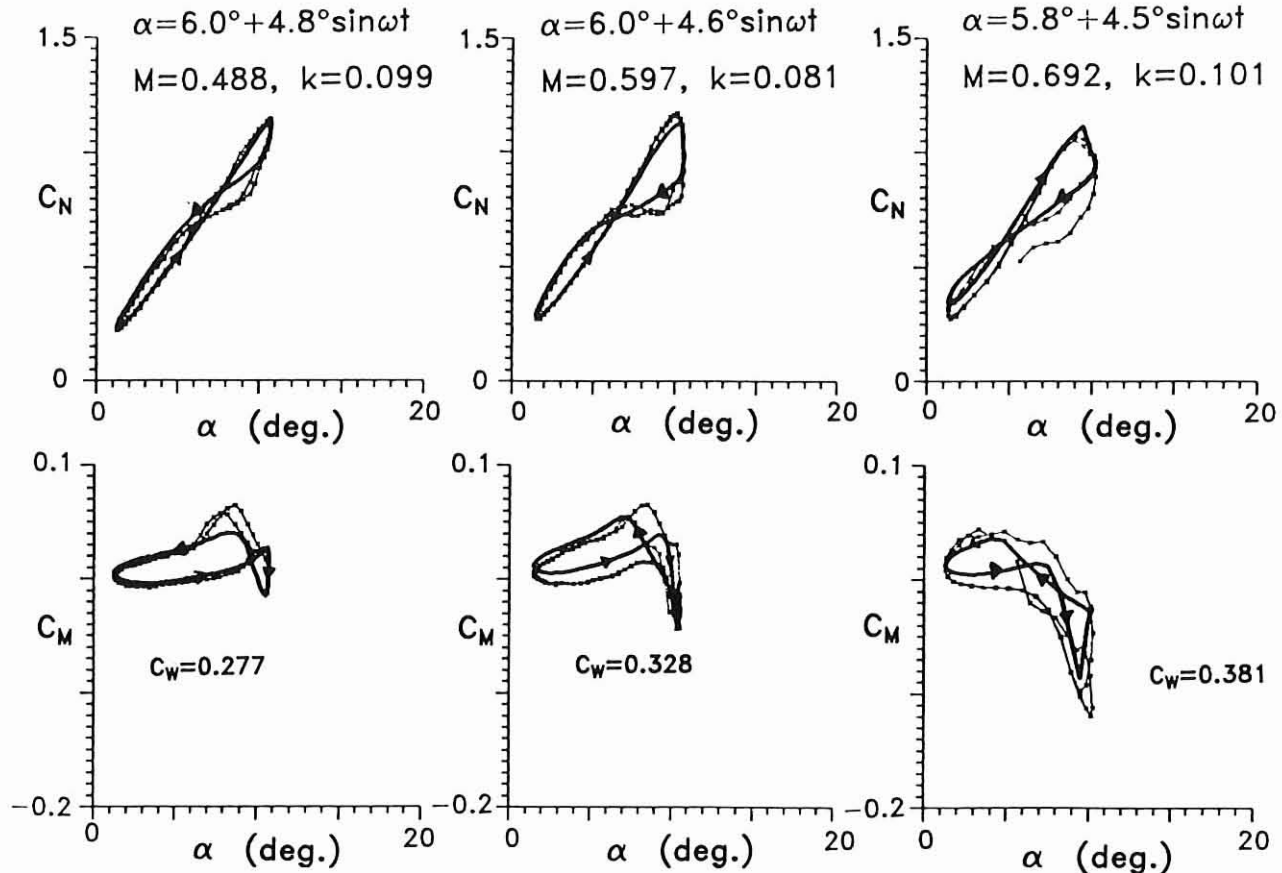


Fig. 12 Example of the effects of increasing Mach number on the airloads during dynamic stall.

Acknowledgments

The research work described in this paper has been funded by the Procurement Executive, U.K. Ministry of Defence. Mr. Peter Wilby, Superintendent of the Structures Department at the Royal Aircraft Establishment, Farnborough, was the technical monitor. Some aspects of the work in this paper were conducted by the first author with the financial support of the U.S. Army Research office under contract DAAL-03-88-C-002. The first author also wishes to thank colleagues at both Westland Helicopters and the University of Maryland for their helpful discussions.

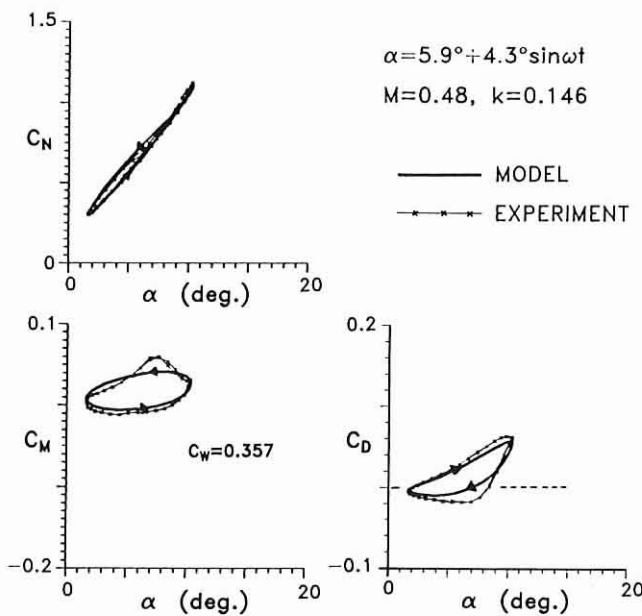


Fig. 13 Suppression of flow separation by increasing the reduced frequency.

References

- ¹Martin, J. M., Empey, R. W., McCroskey, W. J., Caradonna, F. X., "An Experimental Analysis of Dynamic Stall on an Oscillating Airfoil," *Journal of the American Helicopter Society*, Vol. 19, (1), Jan 1974.
- ²Carta, F. O., "Analysis of Oscillatory Pressure Data Including Dynamic Stall Effects," NASA CR-2394, 1974.
- ³Carr, L. W., McAlister, K. W., McCroskey, W. J., "Analysis of the Development of Dynamic Stall based on Oscillating Airfoil Experiments," NASA TN D-8382, 1977.
- ⁴Carr, L. W., McAlister, K. W., McCroskey, W. J., "Dynamic Stall Experiments on the NACA 0012 Airfoil," NASA TP-1100, 1978.
- ⁵McAlister, K. W., Carr, L. W., "Water Tunnel Experiments on an Oscillating Airfoil," NASA TM 78446, 1976.
- ⁶Beddoe, T. S., "A Qualitative Discussion of Dynamic Stall," AGARD Special Course on Unsteady Aerodynamics, AGARD Report 679, 1979.
- ⁷McCroskey, W. J., "The Phenomenon of Dynamic Stall," NASA TM-81264, 1981.
- ⁸Janakiram, R. D., Sankar, L. N., "Emerging Role of First Principles Based Computational Aerodynamics for Rotorcraft Applications," *Proceedings of the 2nd International Conference on Rotorcraft Basic Research*, College Park, Maryland, Feb 1988.
- ⁹Tuncer, I., Wu, J., Wang, C., "Theoretical and Numerical Studies of Oscillating Airfoils," Paper 89-0021, presented at the 27th Aerospace Sciences Meeting, Reno, Nevada, Jan 9-12, 1989.
- ¹⁰Srinivasan, G. R., McCroskey, W. J., "Navier-Stokes Calculations of Hovering Rotor Flowfields," *AIAA Journal of Aircraft*, Vol. 25, (10), 1988.
- ¹¹Gormont, R. E., "A Mathematical Model of Unsteady Aerodynamics

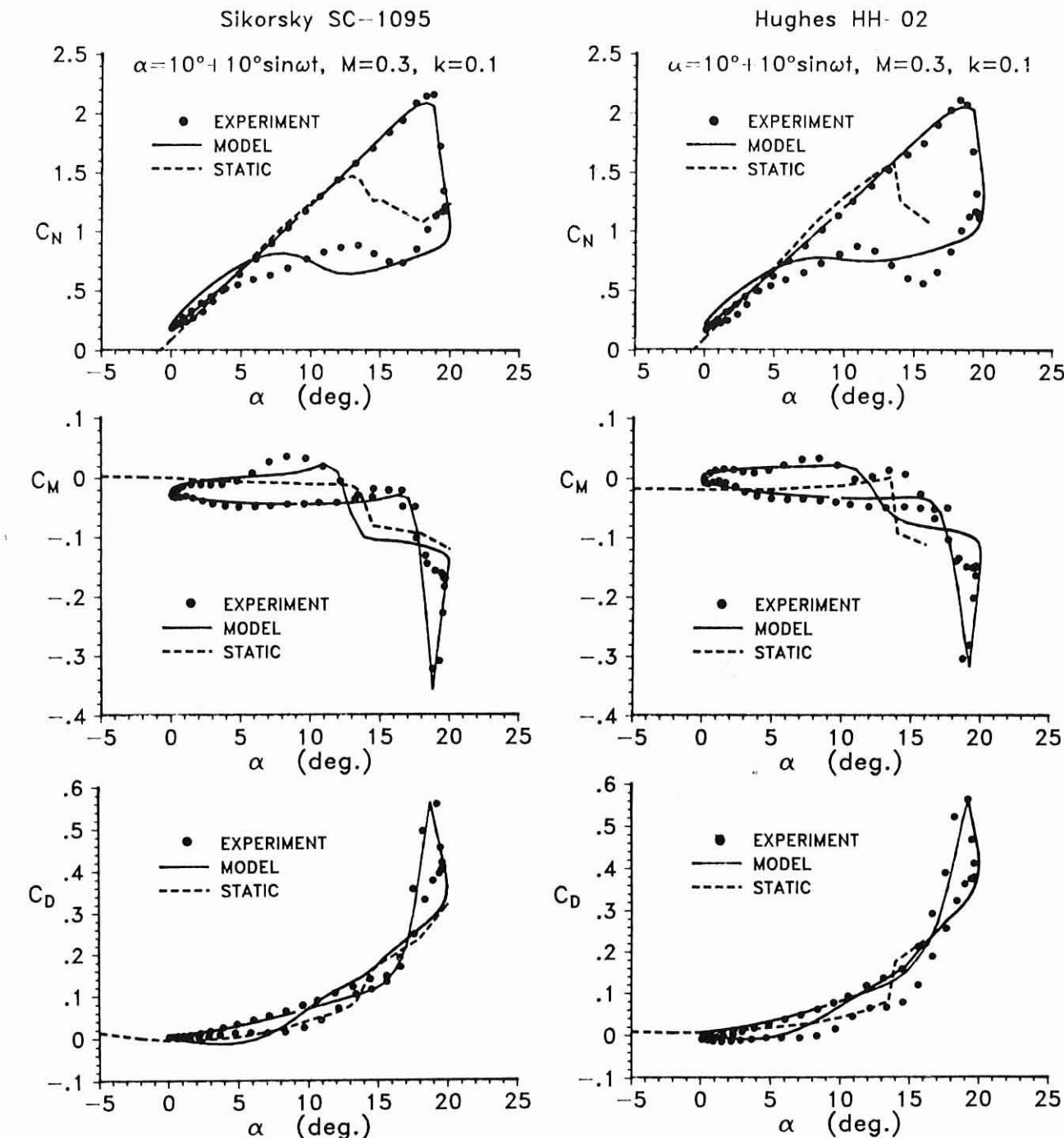


Fig. 14 Prediction of airloads on HH-02 and SC-1095 airfoil sections at $M = 0.3$.

and Radial Flow for the Application to Helicopter Rotor," USAAMRDL Technical Report 72-67, 1973.

¹²Beddoes, T. S., "A Synthesis of Unsteady Aerodynamic Effects Including Stall Hysteresis," *Vertica*, Vol. 1, (2), 1976.

¹³Bielawa, R. L., "Synthesized Airfoil Data Method with Applications to Stall Flutter Calculations," *Proceedings of the 31st Annual Forum of the American Helicopter Society*, 1975.

¹⁴Tran, C. T., Pitot, D., "A Semi-Empirical Model for the Dynamic Stall of Airfoils in View of the Application to the Calculation of Responses of a Helicopter Blade in Forward Flight," *Vertica*, Vol. 5, (1), 1981.

¹⁵Gangwani, S. T., "Synthesized Airfoil Data Method for Prediction of Dynamic Stall and Unsteady Airloads," *Proceedings of the 39th Annual Forum of the American Helicopter Society*, 1983. Also *Vertica*, Vol. 8, 1984.

¹⁶Reddy, T. S. R., Kaza, K. R. V., "A Comparative Study of Some Dynamic Stall Models," NASA TM-88917, 1987.

¹⁷Lomax, H., Heaslet, M. A., Fuller, F. B., Sludder, L., "Two and Three Dimensional Unsteady Lift Problems in High Speed Flight," NACA Report 1077, 1952.

¹⁸Heaslet, M. A., Spreiter, J. R., "Reciprocity Relations in Aerodynamics," NACA Report 1119, Feb 1952.

¹⁹Bisplinghoff, R. L., Ashley, H., Halfman, R. L., *Aeroelasticity*, Addison-Wesley Publishing Co., Reading, Mass., 1955.

²⁰Lomax, H., "Indicial Aerodynamics," AGARD Manual on Aeroelasticity, Part 2, Chapter 6, 1968.

²¹Beddoes, T. S., "Practical Computation of Unsteady Lift," 8th European Rotorcraft and Powered Lift Aircraft Forum, 1982. Also *Vertica*, Vol. 7, (2), 1983.

²²Leishman, J. G., "Validation of Approximate Indicial Aerodynamic Functions for Two-Dimensional Subsonic Flow," *AIAA Journal of Aircraft*, Vol. 25, (10), Oct 1988.

²³Leishman, J. G., Beddoes, T. S., "A Generalized Model for Unsteady

- Airfoil Behavior and Dynamic Stall Using the Indicial Method," *Proceedings of the 42nd Annual Forum of the American Helicopter Society*, Washington D.C., Jun 1986.
- ²⁴Leishman, J. G., "An Analytic Model for Unsteady Drag," *AIAA Journal of Aircraft*, Vol. 25, (7), Jul 1988.
- ²⁵Evans, W. T., Mort, K. W., "Analysis of Computed Flow Parameters for a Set of Sudden Stalls in Low Speed Two-Dimensional Flow," NACA TND-85, 1959.
- ²⁶Beddoes, T. S., "Onset of Leading Edge Separation Effects Under Dynamic Conditions and Low Mach Number," *Proceedings of the 34th Annual Forum of the American Helicopter Society*, 1978.
- ²⁷Beddoes, T. S., "Representation of Airfoil Behavior, AGARD Specialists Meeting on the Prediction of Aerodynamic Loads on Rotorcraft," AGARD CP-334, 1982. Also *Vertica*, Vol. 7, (2), 1983.
- ²⁸McCroskey, W. J., McAlister, K. W., Carr, L. W., Pucci, S. L., "An Experimental Study of Dynamic Stall on Advanced Airfoil Sections," Vols. 1, 2 & 3 NASA TM-84245, 1982.
- ²⁹Wilby, P. G., "An Experimental Investigation on the Influence of a Range of Airfoil Design Features on Dynamic Stall Onset," Paper No. 2, 10th European Rotorcraft Forum, The Hague, The Netherlands, Aug 28-31, 1984.
- ³⁰Thwaites, B. (ed.), *Incompressible Aerodynamics*, Oxford University Clarendon Press, 1960.
- ³¹Woods, L. C., *The Theory of Subsonic Plane Flow*, Cambridge University Press, 1961.
- ³²Scruggs, R. M., Nash, J. F., Singleton, R. E., "Analysis of Dynamic Stall using Unsteady Boundary Layer Theory," NASA CR-2426, Oct 1974.
- ³³Liiva, J., Davenport, F. J., Grey, L., Walton, I. C., "Two-Dimensional Tests of Airfoils Oscillating Near Stall," USAAVLABS TR-68-13, 1968.
- ³⁴McCroskey, W. J., McAlister, K. W., Carr, L. W., Pucci, S. K., Lambert, O., Indergand, R. F., "Dynamic Stall on Advanced Airfoil Sections," *Proceedings of the 36th Annual Forum of the American Helicopter Society*, Washington DC, May 1980.